An Efficient Motion-Resistant Method for Wearable Pulse Oximeter

Yong-Sheng Yan and Yuan-Ting Zhang, *Fellow, IEEE*

***Abstract*—Reduction of motion artifact and power saving are crucial in designing a wearable pulse oximeter for long-term telemedicine application. In this paper, a novel algorithm, minimum correlation discrete saturation transform (MCDST) has been developed for the estimation of arterial oxygen saturation (S_aO_2), based on an optical model derived from photon diffusion analysis. The simulation shows that the new algorithm MCDST is more robust under low SNRs than the clinically verified motion-resistant algorithm discrete saturation transform (DST). Further, the experiment with different severity of motions demonstrates that MCDST has a slightly better performance than DST algorithm. Moreover, MCDST is more computationally efficient than DST because the former uses linear algebra instead of the time-consuming adaptive filter used by latter, which indicates that MCDST can reduce the required power consumption and circuit complexity of the implementation. This is vital for wearable devices, where the physical size and long battery life are crucial.**

***Index Terms*—Blood oxygen saturation, motion artifact, photoplethysmography (PPG), pulse oximetry, telemedicine, wearable medical device.**

I. Introduction

WEARABLE medical devices are capable of continuously monitoring an individual's vital signs in real time. These devices are particularly important to the world's increasingly aging population, whose health conditions have to be assessed regularly or monitored continuously. In order to make wearable devices practical, a series of technical problems have to be solved. For example, these devices need to be miniature in size, must possess a user-friendly interface, be efficient in power consumption, and be motion resistant when monitoring the vital signs under normal daily life.

The pulse oximeter has been widely used for measuring blood oxygen saturation (SpO_2) in clinical situation. Reduction of motion artifact and power saving are crucial in designing a wearable pulse oximeter for long-term telemedicine application. Actually, a number of attempts have been made in the past decade to improve the accuracy of pulse oximeter when subjects move [1]–[8]. The typical method is based on an independent measure of motion. For example, one or more transducers (e.g., piezo or optical sensors) are employed to record the user's motion. By assuming that the artifact is a linear addition to the pulsatile photoplethysmography (PPG) signal, the original signal can be reconstructed from the corrupted signal [6], [7]. This hypothesis is, however, often doubted when inspecting PPG signals under typical artifact-producing forces [8]. This observation drives researchers to develop more realistic models for the PPG signal or the artifact.

A recently reported motion-resistant algorithm, developed by Masimo called discrete saturation transform (DST), is able to detect the SpO_2 during low perfusion and motion using an adaptive filter based on the Masimo pulse oximetry model derived from Beer–Lambert law [9], [10]. A number of studies have demonstrated that the technique may have a significantly lower failure rate and a lower false positive alarm rate than conventional techniques [9]–[13].

However, some researchers reported that the accuracy of Masimo pulse oximeter deteriorated at deep hypoxia levels (e.g., $S_aO_2 \leq 80\%$) compared to its performance at higher S_aO_2, like common pulse oximeters [3]. The phenomenon can be partly explained by the results of previous theoretical studies based on the photon diffusion analysis, which suggests that changes in physiological factors (i.e., hematocrit, arterial venous saturation differences, etc.) that affect tissue scattering and absorption can significantly affect the accuracy of the pulse oximeters, especially at low S_aO_2 levels [14], [15]. The derived pulse oximeter model from photon diffusion theory, which accounts for both effects of tissue scattering and absorption, has been proven to be a valuable tool to predict the response of pulse oximeter.

In this paper, based on the model derived from photon diffusion analysis, we propose a novel time-efficient algorithm, minimum correlation discrete saturation transform (MCDST), for motion-resistant measurement of SpO_2. Section II describes the principle of the conventional pulse oximeter and the proposed motion-resistant algorithm MCDST. Section III presents the simulation results of S_aO_2 estimation by MCDST, as well as DST algorithm. Section IV presents the experiment results. Finally, Section V gives the discussion and conclusion.

II. Methodology

A. Conventional Pulse Oximetry

The traditional algorithms for estimating SpO_2 detect peaks and troughs of the PPG signal in the time domain. Based on the Beer–Lambert law, which relates the optical path length and effective absorbance to the intensity of transmitted light, the relationship between intensity of transmitted light and SpO_2 is commonly described as

$$I(\lambda, t) = I_0(\lambda)\ \exp[(-s\varepsilon_{\mathrm{HbO_2}}(\lambda) + (1-s)\varepsilon_{\mathrm{Hb}}(\lambda))cd(t)] \quad (1)$$

Manuscript received December 6, 2005; revised December 5, 2006. This work was supported in part by the Hong Kong Innovation and Technology Fund, in part by Standard Telecommunications Ltd., and in part by Jetfly Technology Ltd.

The authors are with the Joint Research Centre for Biomedical Engineering, Department of Electronic Engineering, The Chinese University of Hong Kong, Hong Kong (e-mail: ysyan@ee.cuhk.edu.hk; ytzhang@ee.cuhk.edu.hk).

Color versions of one or more of the figures in this paper are available online at http://ieeexplore.ieee.org.

Digital Object Identifier 10.1109/TITB.2007.902173

where $\varepsilon_{\mathrm{HbO}_2}$ and $\varepsilon_{\mathrm{Hb}}$ are the extinction coefficients of oxygenated and deoxygenated hemoglobin, and s, c, and d represent SpO_2, total concentration of hemoglobin, and the optical path length, respectively.

By using two light sources—red (RD) and infrared (IR) lights—and calculating a normalized ratio of the ac component to the dc component for each light source, SpO_2 can be computed from the ratio of ratios R, i.e., the normalized ratio of the red to the infrared transmitted light intensity. That is

$$R = \frac{(I_{\mathrm{ac}}/I_{\mathrm{dc}})_{\mathrm{RD}}}{(I_{\mathrm{ac}}/I_{\mathrm{dc}})_{\mathrm{IR}}} = \frac{(I_{\mathrm{RD}}/I_{\mathrm{IR}})_{\mathrm{ac}}}{(I_{\mathrm{RD}}/I_{\mathrm{IR}})_{\mathrm{dc}}} \tag{2}$$

and

$$s = \frac{\varepsilon_{\mathrm{Hb}}(\lambda_R) - \varepsilon_{\mathrm{Hb}}(\lambda_{\mathrm{IR}})R}{\varepsilon_{\mathrm{Hb}}(\lambda_R) - \varepsilon_{\mathrm{HbO}_2}(\lambda_R) + [\varepsilon_{\mathrm{HbO}_2}(\lambda_{\mathrm{IR}}) - \varepsilon_{\mathrm{Hb}}(\lambda_{\mathrm{IR}})]R}. \tag{3}$$

By calculating the ratio of the ac components and the ratio of the dc components of the two light sources, SpO_2 can be obtained from every single pulse of a PPG signal. To stabilize the reading, the weighted moving average (WMA) is often used [5], [16]. Typical averaging methods, e.g., the median averaging and standard arithmetic averaging, are applied to every several samples or samples in every several second intervals.

B. MCDST Algorithm

Although the operation of pulse oximeters can be understood qualitatively using an analysis based on Beer–Lambert law, this approach fails to account for the effects of intense scattering of light in tissue [14], [15]. In this paper, we employ photon diffusion theory to derive the pulse oximeter model relating to the finger motion (see the Appendix). The model has the same form as the Masimo pulse oximetry model [10] except the different ratio of ratios R_a

$$\begin{aligned} \mathrm{RD} &= R_a S + R_v N \\ \mathrm{IR} &= S + N \end{aligned} \tag{4}$$

where RD and IR represent normalized red and infrared light intensity, S and N are the pulsatile component and motion artifact, and R_a and R_v are the ratio of ratios relating to $\mathrm{S_aO_2}$ and venous blood oxygen saturation ($\mathrm{S_vO_2}$), respectively.

Based on this model, a novel algorithm, MCDST, is proposed using a subspace-based technique for $\mathrm{S_aO_2}$ estimation from motion-corrupted signals.

With the assumption that the pulsatile component (S) is uncorrelated with motion artifact (N), the inner product $\langle S,\ N\rangle$ can be neglected compared with the inner product $\langle S,\ S\rangle$ and $\langle N,\ N\rangle$. Then, the constrained relationship between R_a and R_v could be found roughly by solving the following equations:

$$\begin{cases} A_{11} \equiv \langle \mathrm{IR}, \mathrm{IR}\rangle = \langle S,S\rangle + \langle N,N\rangle + 2\langle S,N\rangle \\ \qquad \approx \langle S,S\rangle + \langle N,N\rangle \\ A_{22} \equiv \langle \mathrm{RD}, \mathrm{RD}\rangle = R_a^2\langle S,S\rangle + R_v^2\langle N,N\rangle + 2R_aR_v\langle S,N\rangle \\ \qquad \approx R_a^2\langle S,S\rangle + R_v^2\langle N,N\rangle \\ A_{12} \equiv \langle \mathrm{IR}, \mathrm{RD}\rangle = R_a\langle S,S\rangle + R_v\langle N,N\rangle + (R_a+R_v)\langle S,N\rangle \\ \qquad \approx R_a\langle S,S\rangle + R_v\langle N,N\rangle \end{cases} \tag{5}$$

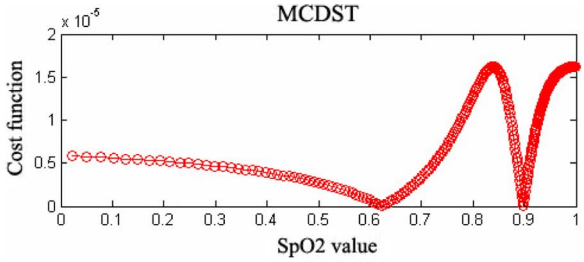

Fig. 1. Illustration of the MCDST spectrum. The local minimums represent $\mathrm{S_aO_2}$ and $\mathrm{S_vO_2}$ values corresponding to the ratios R_a and R_v.

where A_{11}, A_{22}, and A_{12} can be calculated directly according to the normalized ac component of received PPG signal, respectively. Solving (5), we get

$$R_a = \frac{A_{22} - A_{12}R_v}{A_{12} - A_{11}R_v}. \tag{6}$$

It means that the discrete choice of R_a will simultaneously determine the value of R_v.

Choosing the value of r_a stepping through a range of 0–100% of $\mathrm{S_aO_2}$ [the corresponding value of r_v can be calculated using (6)], the reference pulsatile signal and noise are generated by

$$\begin{aligned} \mathrm{RS} &= r_v\mathrm{IR} - \mathrm{RD} \\ \mathrm{RN} &= r_a\mathrm{IR} - \mathrm{RD}. \end{aligned} \tag{7}$$

With the different pair of reference signals generated, a subspace-based technique was used to identify R_a and R_v based on the minimum correlation between S and N. For the two vectors or subspaces RS and RN, the angle between them is defined as $\cos^{-1}(\mathrm{RS}' \times \mathrm{RN})$. The angle is a good indicator of independence or correlation. For example, if the angle between the two subspaces is small, the two spaces are nearly linearly dependent. In our study, based on the assumption that S and N are independent, the angle between the two subspaces RS and RN will be nearest to $\pi/2$ when $r_a = R_a$ or $r_v = R_v$. To stabilize the optimization process, we construct a cost function considering not only the equal time dependence but also the time-delayed dependence between the subspaces

$$\begin{aligned} T = {} & \mathrm{abs}\left[\mathrm{angle}(\mathrm{RS}(t), \mathrm{RN}(t)) - \pi/2\right] \\ & + \sum_{\tau=1,\ \ldots,\ n} \mathrm{abs}\left[\mathrm{angle}(\mathrm{RS}(t), \mathrm{RN}(t+\tau)) - \pi/2\right]. \end{aligned} \tag{8}$$

Here, the function $\mathrm{angle}(x, y)$ finds the angle between two subspaces specified by the columns of x and y, the parameter τ is selected from $N = 1$ to $N = 20$ in this study, which is an approximate number of points in one period of PPG signal. As the value of r is chosen discretely according to the limited saturation level 0–100%, the optimization problem of minimizing (8) could be easily solved with stepping through all the possibilities. The ratios R_a and R_v will occur at the local minimums in the MCDST spectrum (Fig. 1).

In summary, the MCDST algorithm comprises the following steps.

1) Collect the red and infrared signals, and calculate the normalized pulsatile component of either signal.

2) Calculate the constrained relationship between R_a and R_v.
3) Synthesize the reference pulsatile signal and motion artifact for each discrete S_aO_2 level in the range 0–100% based on (7), and compute the cost function (8) as well.
4) Obtain the MCDST spectrum and identify the local minimums in the spectrum to determine the values of S_aO_2 and S_vO_2.

In contrast to DST algorithm that detects the optimal R_a and R_v using an adaptive filter, MCDST detects the optimal pair of R_a and R_v.

III. Simulation

The performance of the proposed algorithm MCDST, as well as the clinical verified algorithm DST, was evaluated in simulation. The motion artifact contaminated PPG signal was synthesized by 1-Hz sine wave with bandpass (0.5–3 Hz) filtered white normal distributed noise. The SNR was defined as

$$\text{SNR} = \sqrt{\frac{\text{var}(S)}{\text{var}(N)}} \tag{9}$$

where var(S) and var(N) are the variance of the signal S and N. A set of synthesized signals with different SNRs could be obtained by changing the amplitude of filtered white noise. The S_aO_2 and S_vO_2 were predetermined as 90 and 65%.

A. S_aO_2 Estimation

Fig. 2(a) shows the simulated RD and IR PPG signals under the condition of slight motion artifacts (SNR $= 3$ dB). The corresponding DST and MCDST spectrums are depicted in Fig. 2(b). Clearly, the power curve derived from DST has a sharp peak at saturation $= 90\%$ and a smaller peak at saturation $= 67\%$, which reveals that DST has the ability of identifying the S_aO_2 as well as S_vO_2 during the slight motion trial. The similar phenomena was found for the MCDST spectrum that there are two obvious local minimums at saturation $= 90$ and 64%, which indicates that MCDST can also accurately detect both S_aO_2 and S_vO_2. Actually, with the increasing SNR, the peak near 65% in DST spectrum disappears prior to the corresponding minimum point in MCDST spectrum. It indicates that MCDST may be more powerful to detect S_vO_2 than DST under slight motion conditions.

Similarly, Fig. 3(a) shows the simulated RD and IR PPG signals under the condition of severe motion artifacts (SNR $= -10$ dB). The corresponding DST and MCDST spectrums are depicted in Fig. 3(b). The DST power curve shows two peaks at saturation level 65 and 85%, corresponding to S_vO_2 and S_aO_2, respectively. Clearly, the DST can detect an accurate S_vO_2, but a biased (5%) S_aO_2 because the motion noise (N) is much bigger than the pulsatile signal (S). However, the MCDST spectrum can detect both the S_vO_2 (66%) and S_aO_2 (90%) accurately under such a severe motion condition.

Fig. 4 gives the absolute S_aO_2 estimation errors (the absolute value of the estimated S_aO_2 minus referenced S_aO_2) of DST and MCDST algorithms based on the motion contaminated signals with different SNRs. It is found that MCDST outperforms DST under the severe motion conditions (i.e., low SNR), but demonstrates a comparable performance under the modest motion conditions (relatively higher SNR).

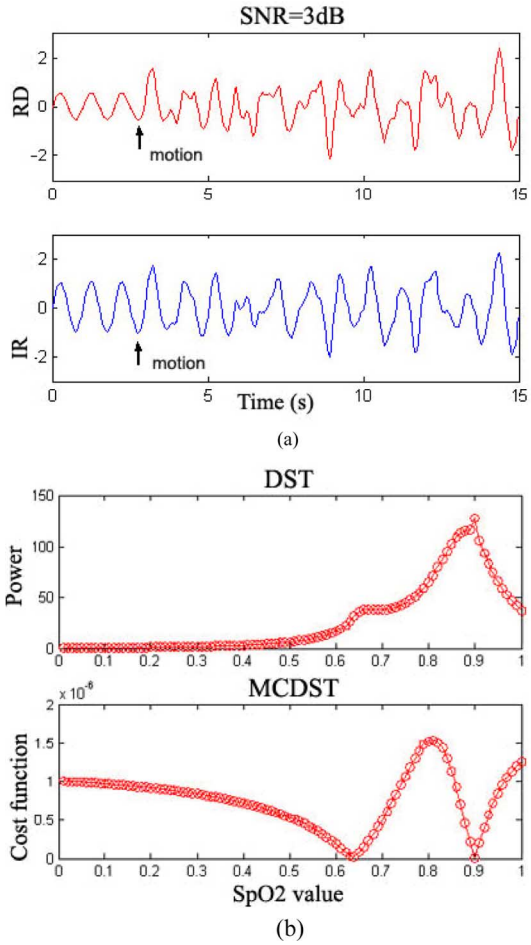

Fig. 2. (a) Simulated RD and IR PPG signals and (b) corresponding DST and MCDST spectrums under motion condition (SNR $= 3$ dB). The S_aO_2 and S_vO_2 were predetermined as 90% and 65%.

B. Computational complexity

As the authors didn't clarify the adaptive filter used in [9]–[11], in order to implement the DST, the adaptive algorithm for the adaptive filter has to be chosen in this study. The common adaptive algorithms include the least-mean square (LMS) algorithm and the recursive least-square (RLS) algorithm. The LMS algorithm is based on the approximation of the steepest decent method. It is widely used because of simplicity, but it has a very slow convergence rate and is not applicable to the fast time-varying signals, i.e., motion artifact in this study. The RLS algorithm, as an exact solution of optimal filter for given signals, has a much faster convergence rate than LMS algorithm. But the limitation is that the conventional RLS algorithm requires $O(M^2)$ operations while the LMS only requires $O(M)$ operations, where M is the taps of the adaptive filter.

In this study, we examine the implementation of DST with the "fast RLS"—QR-decomposition-based least-squares lattice

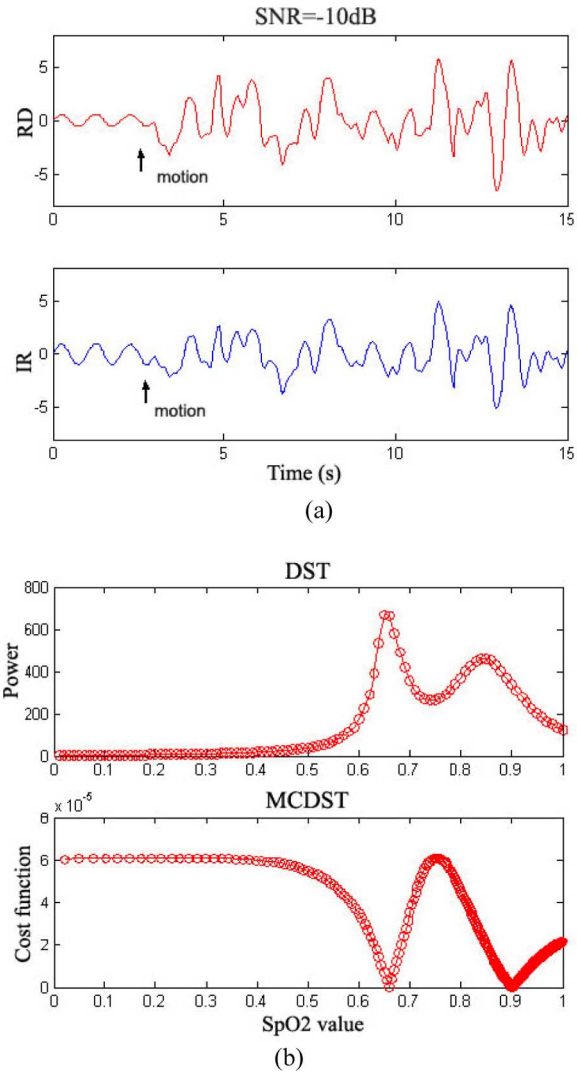

Fig. 3. (a) Simulated RD and IR PPG signals and (b) corresponding DST and MCDST spectrums under motion condition (SNR $= -10$ dB). The S_aO_2 and S_vO_2 were predetermined as 90% and 65%.

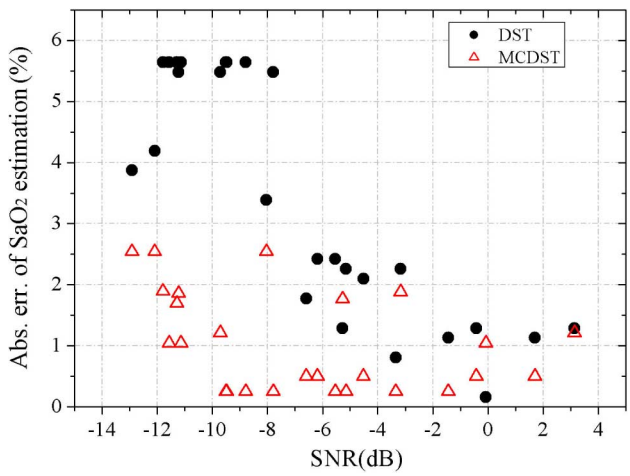

Fig. 4. Absolute S_aO_2 estimation errors of DST (circles) and MCDST (triangles) algorithms based on the motion contaminated signals with different SNRs.

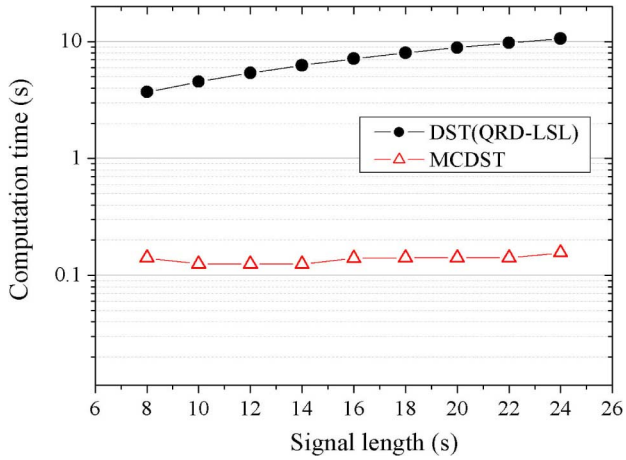

Fig. 5. Computation time of DST with QRD-LSL adaptive filter (circles) and MCDST (triangles) versus the tested signal lengths.

(QRD-LSL) algorithms, which actually represent an alternative to LMS algorithms in many applications due to their fast convergence and good numerical stability. The QRD-LSL (based on given rotations) only needs $O(M)$ operations per time instance as compared to $O(M^2)$ for the conventional RLS algorithm [17].

The simulation is implemented in PC with MATLAB7.0. The SNR is 0 dB, and the taps of adaptive filter is $M = 32$, which makes DST derive as good result of S_aO_2 estimation as that from the MCDST. Fig. 5 gives the computation time of DST with QRD-LSL adaptive filter and MCDST versus the tested signal lengths, respectively. It shows that the computation time of DST significantly increases (from 3.7 to 10.6 s) with the increased signal length (from 8.0 to 24 s), as compared to that of MCDST (from 0.12 to 0.15 s). Here, the minimum 8 s signal length is selected in order to satisfy clinical requirements for S_aO_2 estimation [18], [19]. It is obvious that MCDST is much more computational efficient than DST, which indicates that MCDST can reduce the required power consumption, as well as circuit complexity of the implementation. It is of vital importance for wearable devices, where the physical size and long battery life are crucial.

In summary, the simulation results suggest that the MCDST has a better performance than the DST for S_aO_2 estimation under severe motion artifact due to its detection of the optimal pair of ratios. Moreover, the MCDST is more computationally efficient than the DST because it is based on linear algebra instead of an adaptive filter used in the DST, which makes it more suitable for the applications in wearable devices.

IV. Experiments

A. Experiment protocol

The aim of this experiment is to verify the MCDST algorithm and compare the performance of the MCDST in estimating S_aO_2 on subjects in a resting position and in motion with the conventional WMA algorithm and motion-resistant DST algorithm. Six healthy subjects participated in the study. Four kinds of motions have been investigated and classified into three categories:

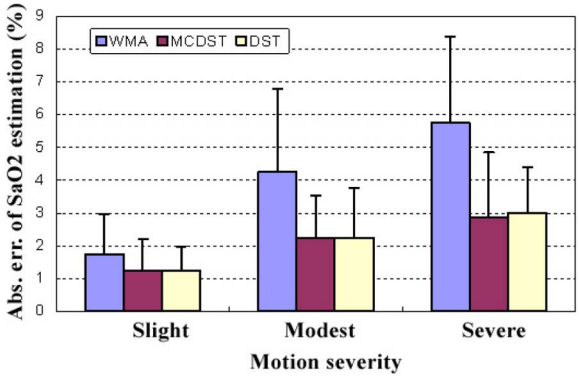

Fig. 6. Absolute S_aO_2 estimation errors (mean and standard deviation) of different algorithms. WMA (gray bar), MCDST (dark gray bar), and DST (light gray bar) under the slight, modest, and severe motions of the finger and/or hand.

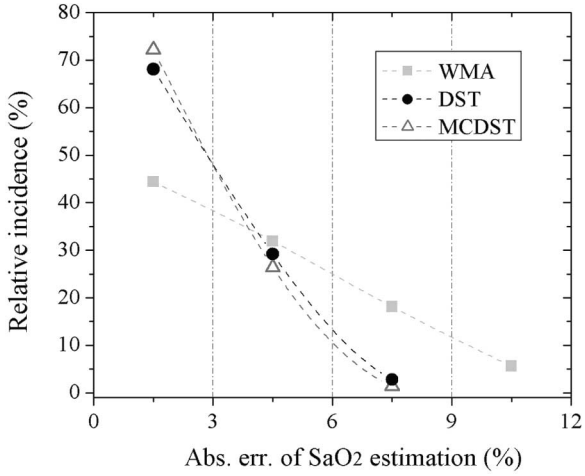

Fig. 7. Distribution of the absolute S_aO_2 estimation errors of different algorithms. WMA (squares), DST (circles), and MCDST (triangles) for all the tested motions.

1) slight motions (random horizontal and vertical motions of the hand), 2) modest motions (changing the contact force during monitoring by pressing the sensor), and 3) severe motions (finger bending). These motions were selected because they are some of the common movements attributable to the motion artifact in pulse oximetry [20], [21]. Subjects were asked to perform all four movements, four times each, and each time for a duration of 30 s. When performing each movement, subjects were asked to move their right hand, or the index finger of their right hand, for a magnitude of 2–5 cm at a frequency of 0.5–4 Hz, while keeping their left hand stationary. The reference signals were recorded from the motionless left hand immediately after each trial with same sensor.

The collected signals were separated into an ac and dc component. The ac component was extracted using a 64th-order FIR bandpass filter with cutoff frequencies at 0.5 and 20 Hz. Throughout the analysis, the reference S_aO_2 was estimated by WMA algorithm as there was little difference between the outputs from different algorithms for the reference motionless hands.

B. Results

Fig. 6 gives the absolute S_aO_2 estimation errors of different algorithms (WMA, MCDST, and DST) under the slight, modest, and severe motions of the finger and/or hand, respectively. It is clear that both DST and MCDST can reduce the S_aO_2 estimation errors during motions, compared with the result from WMA algorithm. But the MCDST does not outperform the DST substantially as expected in simulation. In addition, slight motions, induced by vertical and horizontal movements of hand, cause smaller errors rather than relatively severe motions, which is consistent with the simulation results.

Fig. 7 shows the distribution of the absolute S_aO_2 estimation errors of different algorithms (WMA, DST, and MCDST) for all the tested motions. It is found that the estimation error of the MCDST algorithm have a higher incidence (72%) in the smaller error band ($<3\%$), which is the range of bias commonly accepted by most pulse oximeter manufacturers, as compared to those of the DST (68%) and WMA (44%) algorithms. In other words, the S_aO_2 errors obtained by the MCDST algorithm are more concentrated in the region of smaller errors. In general, the MCDST outperforms WMA and shows a comparable concentration to the DST.

V. Discussion and Conclusion

A pulse oximeter model derived from photon diffusion analysis has been proposed taking account of motion artifact. By virtue of its ability to describe both tissue scattering and absorption effects, the model may help to reduce the errors of S_aO_2 estimation at relatively lower oxygen saturation levels, where the accuracy of the estimation is substantially affected by the changes of physiological factors, such as hematocrit. But it needs to be further examined with clinical experiments in the near future.

Based on the model, the new algorithm MCDST uses time and time-delayed independence between the interested pulsatile component and motion-induced noise to enable motion-resistant detection of S_aO_2. The feasibility and efficacy of this algorithm were verified with different severity of motions, compared with the clinically verified DST algorithm.

The simulation results show that the MCDST is more robust to detect S_aO_2 in low SNRs than the DST. It is not observed in the experiment with finger motions. It may be because the lowest SNR found in the experiment was above -4 dB, in which range, the performance for DST and MCDST in simulation is still comparable. Another possible reason is that the Gaussian noise assumption of motion artifact in simulation is not strongly supported in practice. Nevertheless, the MCDST is still applicable to motion-resistant S_aO_2 estimation because it performs at least as well as the DST algorithm. It should be noted that we did not compare the estimated S_aO_2 with the "true" S_aO_2 level, which is usually obtained by analyzing the blood sample using CO-oximeter. However, it is enough to evaluate the performance of different approaches in motion artifact reduction with the relative S_aO_2 changes.

In addition, the MCDST is more computationally efficient than the DST because the former uses linear algebra instead of

time-consuming adaptive filter used by the latter, which indicates that the MCDST can reduce the required power consumption and circuit complexity of the implementation. It is vitally important for portable or wearable devices, where the small physical size and long battery life are crucial.

This paper focuses on the comparison of DST and MCDST algorithms in offline implementation. Compared to offline implementation, the performance of a real-time system will be influenced by more issues such as other relevant motion-resistant algorithms running in a parallel mode and different digital processing resources, namely, the computational capability provided by the onboard digital signal processors (DSP). As a result, it might cause some difficulty in comparing the targeted algorithms. However, it is very important to take into account those practical issues for developing a clinically useful pulse oximeter. Thus, future research will focus on incorporating the proposed MCDST algorithm in a real pulse oximeter for further performance comparison with Masimo instrument at the system level using the approach proposed in [22].

It should be noted that the sensor used in this paper may be lack of perfect mechanic design to satisfy the model. As a result, the efficacy of motion artifact reduction may not be as good as expected. That is why, we did not directly compare the experimental results with the reported result of Masimo DST algorithm [11]–[13]. A variety of solutions to the issue of good mechanic design of probe may form the core of further work.

APPENDIX

Based on the photon diffusion analysis, the normalized first derivative of the received light intensity is [15]

$$\frac{\Delta I}{I} = \frac{dI/dt}{I} = -\frac{3\Sigma_s d}{2} K(\alpha, d) \sum_a^{\text{art}} \frac{dV_a}{dt} \tag{10}$$

where V_a and $\Sigma_{\text{a}}^{\text{art}}$ are the volume fractions and absorption coefficients of arterial blood, respectively. $K(\alpha, d)$ is a function of the attenuation coefficient α and of the finger thickness d.

With finger movements, the venous blood in the vascular bed is more easily deformed because the venous blood has a lower pressure than the arterial blood pressure. Therefore, the normalized first derivative of the received light intensity becomes

$$\frac{\Delta I}{I} = \frac{dI/dt}{I} = -\frac{3\Sigma_s d}{2} K(\alpha, d) \left(\sum_a^{\text{art}} \frac{dV_a}{dt} + \sum_a^{\text{ven}} \frac{dV_v}{dt} \right). \tag{11}$$

Therefore, the normalized first derivatives for both red and infrared lights are obtained as

$$\begin{aligned} \text{RD} &= \frac{dI/dt}{I} \\ &= -\frac{3\Sigma_s(\text{r}) d}{2} K(\alpha_r, d) \left(\sum_a^{\text{art}} (r) \frac{dV_a}{dt} + \sum_a^{\text{ven}} (r) \frac{dV_v}{dt} \right) \\ &= R_a S + R_v N \\ \text{IR} &= \frac{dI/dt}{I} \\ &= -\frac{3\Sigma_s(\text{ir}) d}{2} K(\alpha_{ir}, d) \left(\sum_a^{\text{art}} (ir) \frac{dV_a}{dt} + \sum_a^{\text{ven}} (r) \frac{dV_v}{dt} \right) \\ &= S + N \end{aligned} \tag{12}$$

where

$$R_a \equiv \frac{K(\alpha_r, d)\Sigma_a^{\text{art}}(r)\Sigma_{\text{s}}(r)}{K(\alpha_{ir}, d)\Sigma_a^{\text{art}}(ir)\Sigma_s(\text{ir})}$$

$$R_v \equiv \frac{K(\alpha_r, d)\Sigma_a^{\text{ven}}(r)\Sigma_s(r)}{K(\alpha_{ir}, d)\Sigma_a^{\text{ven}}(ir)\Sigma_s(\text{ir})}$$

and RD and IR represent normalized red and infrared light intensity, S and N are the pulsatile component and motion artifact, respectively.

Then, the relationship between R and arterial blood oxygen saturation (s) that results from photon diffusion analysis could be expressed as [15]

$$s = \frac{\varepsilon_{\text{Hb}}(\lambda_R) - \varepsilon_{\text{Hb}}(\lambda_{\text{IR}}) \frac{R_a}{K'}}{[\varepsilon_{\text{Hb}}(\lambda_R) - \varepsilon_{\text{HbO}_2}(\lambda_R)]K' + [\varepsilon_{\text{HbO}_2}(\lambda_{\text{IR}}) - \varepsilon_{\text{Hb}}(\lambda_{\text{IR}})] \frac{R_a}{K'}} \tag{13}$$

where

$$K' = \frac{K(\alpha_r, d)\Sigma_{\text{s}}(r)}{K(\alpha_{ir}, d)\Sigma_{\text{s}}(\text{ir})}$$

and $\varepsilon_{\text{HbO}_2}$ and ε_{Hb} are the extinction coefficients of oxygenated and deoxygenated hemoglobin. It is clear that the expression relating R and $\text{S}_{\text{a}}\text{O}_2$ derived from photon diffusion analysis (13) is not only dependent on the extinction coefficients of hemoglobins, but also on the optical properties of the tissue medium and geometrical constants. However, the well-known relationship between arterial oxygen saturation and the ratio r derived from Beer–Lambert's law is completely dependent on the extinction coefficients of hemoglobins, as expressed in (3).

REFERENCES

[1] A. R. Visram, R. D. M. Jones, M. G. Irwin, and J. Bacon-Shone, "Use of two pulse oximeters to investigate a method of movement artifact rejection using photo-plethysmographic signals," *Brit. J. Anaesth.*, vol. 72, pp. 388–392, 1994.

[2] W. B. Runciman, R. K. Webb, L. Barker, and M. Curriie, "The pulse oximeter: Application and limitations: An analysis of 2000 incident reports," *Anaesth. Intensive Care*, vol. 21, pp. 543–550, 1993.

[3] F. A. Robertson, G. M. Hoffman, E. A. Stuth, S. Staudt, and R. Berens, "In vivo evaluation of Masimo SET and Nellcor N-395 oximetry accuracy compared to CO-oximetry in chronically desaturated children," *Anesthesiology*, vol. 99, p. A620, 2003.

[4] R. Sokwoo, B. H. Yang, and H. H. Asada, "Artifact-resistant power-efficient design of finger-ring plethysmographic sensors," *IEEE Trans. Biomed. Eng.*, vol. 48, no. 7, pp. 795–805, Jul. 2001.

[5] Y. S. Yan, C. C. Poon, and Y. T. Zhang, "Reduction of motion artifact in pulse oximetry by smoothed pseudo Wigner–Ville distribution," *J. Neuroeng. Rehabil.*, vol. 2, no. 1, p. 3, Mar. 1, 2005.

[6] M. K. Diab, "Signal processing apparatus," International Patent Application WO 96/12435, May 2, 1996.

[7] D. Parker, "Optical monitor (oximeter, etc.) with motion artifact suppression," International Patent Application WO 94/03102, Feb. 17, 1994.

[8] M. J. Hayes and P. R. Smith, "Artifact reduction in photoplethysmography," *Appl. Opt.*, vol. 37, pp. 7427–7446, 1998.

[9] C. Dumas, J. A. Wahr, and K. K. Tremper, "Clinical evaluation of a prototype motion artifact resistant pulse oximeter in the recovery room," *Anesth. Analg.*, vol. 83, pp. 269–272, 1996.
[10] J. M. Goldman, M. T. Petterson, R. J. Kopotic, and S. J. Barker, "Masimo signal extraction pulse oximetry," *J. Clin. Monit. Comput*, vol. 16, pp. 475–483, 2000.
[11] P. R. Lichtenthal and L. D. Wade, "Evaluation of signal extraction technology (SET) in preventing false alarms when using pulse oximetry in the recovery room," *Anesthesiology*, vol. 86, pp. 278–279, 1996.
[12] N. S. Trivedi, N. K. Shah, and B. P. Jacobsen, "New pulse oximeter: Resistant to motion artifacts," *Anesth. Analg.*, vol. 80, p. S510, 1995.
[13] N. Shah, S. Barker, and J. Hyatt, "Comparison of alarm conditions between new pulse oximeters during motion at normal and low oxygen saturations," *Anesthesiology*, vol. 83, p. A1067, 1995.
[14] D. R. Marble and P. W. Cheung, "Mathematical model of transmission pulse oximetry," in *Proc. IEEE Eng. Med. Biol. Soc. 10th Annu. Conf.*, New Orleans, LA, 1988, pp. 542–543.
[15] J. M. Schmitt, "Simple photon diffusion analysis of the effects of multiple scattering on pulse oximetry," *IEEE Trans. Biomed. Eng.*, vol. 38, no. 12, pp. 1194–1203, Dec. 1991.
[16] J. G. Webster, *Design of Pulse Oximeters*. Philadelphia, PA: Inst. Phys. Pub., 1997.
[17] F. Ling, "Given rotation based least squares lattice and related algorithms," *IEEE Trans. Signal Process.*, vol. 39, no. 7, pp. 1541–1551, Jul. 1991.
[18] T. L. Rusch, R. Sankar, and J. E. Scarf, "Signal processing methods for pulse oximetry," *Comput. Biol. Med.*, vol. 26, pp. 143–159, 1996.
[19] F. U. Dowla, P. G. Skokowski, and R. R. Leach, "Neural networks and wavelet analysis in the computer interpretation of pulse oximetry data," presented at the IEEE Workshop Neural Netw. Signal Process., Kyoto, Japan, 1996.
[20] R. M. Tobin, J. A. Pologe, and P. R. B. Batchelder, "A characterization of motion affecting pulse oximetry in 350 patients," *Anesth. Analg.*, vol. 94, Suppl. 1, pp. S54–S61, 2002.
[21] S. J. Barker, "Motion-resistant pulse oximetry: A comparison of new and old models," *Anesth. Analg.*, vol. 95, pp. 967–972, 2002.
[22] S. W. Kastle and E. Konecny, "Determining the artifact sensitivity of recent pulse oximeter during laboratory benchmarking," *J. Clin. Monit. Comput*, vol. 16, pp. 509–522, 2000.

Yong-Sheng Yan received the B.S. degree in physics and the M.S. degree in acoustics both from Nanjing University, Nanjing, China, in 1999 and 2002, respectively, and the Ph.D. degree in biomedical engineering from The Chinese University of Hong Kong (CUHK), Hong Kong, SAR, in 2005.

He is currently a Postdoctoral Fellow in the Joint Research Center for Biomedical Engineering, CUHK. His current research interests include biomedical signal processing, and wearable medical devices and biosensors for mobile health.

Yuan-Ting Zhang (M'90–SM'93–F'07) received the Ph.D. degree in biomedical engineering from the University of New Brunswick, Fredericton, NB, Canada, in 1990.

He is currently the Director of the Joint Research Center for Biomedical Engineering and the Head of the Division of Biomedical Engineering at The Chinese University of Hong Kong (CUHK), Hong Kong, SAR. He is also the Director of the Center for Medical Devices at the Shenzhen Institute of Advanced Technology, the Chinese Academy of Science and CUHK, and the Chairman (adjunct) in the Department of Biomedical Engineering, Sun Yat-Sen University, Guangzhou, China. From 1989 to 1994, he was a Research Associate and Adjunct Assistant Professor at the University of Calgary, Calgary, AB, Canada. He Chaired the Biomedical Division of Hong Kong Institution of Engineers during 1996–1997 and 2000–2001. He is an Associate Editor of the *Journal of Neuroengineering and Rehabilitation*. His current research interests include neural engineering, wearable medical devices, and body sensor networks particularly for mobile health and telemedicine. He is the author or coauthor of more than 300 scientific articles published in the area of biomedical engineering.

Dr. Zhang is a Fellow of the International Academy of Medicinal and Biological Engineering (IAMBE), the American Institute for Medical and Biological Engineering (AIMBE). He has been an active member in the IEEE Engineering in Medicine and Biology Society (EMBS). He was the Technical Program Chair of the 20th Annual International Conference in 1998, and the General Conference Chair of the 27th Annual International Conference in 2005. He served as the TPC Chair of the IEEE-EMBS Summer School and Symposium on Medical Devices and Biosensors (ISSS-MDBS) in 2006. He was elected as an AdCom member in 1999 and served as the Vice President (Conferences) in 2000. He has served as an Associate Editor of the IEEE TRANSACTIONS ON BIOMEDICAL ENGINEERING and the IEEE TRANSACTIONS ON MOBILE COMPUTING. He was also the Guest Editor of the IEEE COMMUNICATION MAGAZINE and the IEEE TRANSACTIONS ON INFORMATION TECHNOLOGY IN BIOMEDICINE. He is currently on the Editorial Board of the Book Series of Biomedical Engineering published by the IEEE press, the IEEE-EMBS Technical Committee of Wearable Systems and Sensors, and the Editorial Committee of China Medical Device Information. He is an honorary Advisor to the Hong Kong Medical and Healthcare Device Manufacture Association. He is the recipient of numerous awards and recognitions including the 2006 IEEE-EMBS Service Award.